Laser speckle field as a multiple particle trap

2010 J. Opt. 12 124003

(http://iopscience.iop.org/2040-8986/12/12/124003)

IOP Publishing Journal of Optics

J. Opt. **12** (2010) 124003 (8pp) doi:10.1088/2040-8978/12/12/124003

Laser speckle field as a multiple particle trap

V G Shvedov[1,2,3], A V Rode[1], Ya V Izdebskaya[2,3], D Leykam[2], A S Desyatnikov[2], W Krolikowski[1] and Yu S Kivshar[2]

[1] Laser Physics Centre, Research School of Physics and Engineering, The Australian National University, Canberra ACT 0200, Australia

[2] Nonlinear Physics Centre, Research School of Physics and Engineering, The Australian National University, Canberra ACT 0200, Australia

[3] Department of Physics, Taurida National University, Simferopol 95007 Crimea, Ukraine

E-mail: avr111@physics.anu.edu.au

Received 15 March 2010, accepted for publication 23 September 2010
Published 11 November 2010
Online at stacks.iop.org/JOpt/12/124003

Abstract

We demonstrate that a speckle pattern in the spatially coherent laser field transmitted by a diffuser forms a multitude of three-dimensional intensity micro-pockets acting as particle traps for air-borne light absorbing particles. Confinement of up to a few thousand particles in air with a unidirectional single beam has been achieved. Theoretical analysis of the speckle defined trapping volume is in a good agreement with experimental results on capturing of aggregates of carbon nanoparticles in air.

Keywords: speckle field, optical trapping in air

(Some figures in this article are in colour only in the electronic version)

1. Introduction

Laser trapping, guiding and manipulation of particles have shown remarkable advances in biology and chemistry in the past decade. The progress has come about through the unique ability of laser light to insert a calibrated force of the order on piconewtons or less to microscopic or nanoscale objects in a controllable manner [1–4]. Most of the research and applications of optical trapping were developed for an aqueous medium or/and vacuum using the radiation pressure of light. On the other hand, only a small number of publications have been devoted to trapping and manipulation of absorbing particles in a gaseous environment, and those were mostly concerned with transparent water-based aerosol droplets [5, 6]. The main difficulty is associated with the presence of radiometric forces, which tend to push the particle away from the maximum intensity of the beam. In gases these thermal, or photophoretic, forces are much stronger than the radiation pressure because of much lower heat dissipation when compared to liquids.

The idea of utilizing the inhomogeneous heating of particles in gases with a laser beam to induce photophoretic forces for their trapping was proposed in a number of early works [7–13]. The photophoretic force is caused by the interaction of the molecules of the surrounding gas with the heated particle surface. The gas molecules reflected from a hotter side of the particles acquire higher speed than those reflected from a colder side; as a result the particle acquires a net momentum. In spite of repeated attempts, a reliable long lasting trapping of absorbing particles in air was accomplished only recently in a trap formed by counter-propagating optical vortex beams [14, 15]. The intensity of the electric and magnetic fields of the counter-propagating beams retains the axial distribution symmetry with zero intensity on the common axis, and hence forms a stable potential well for trapping particles. The doughnut-like vortex beam shape [16] provides two-dimensional confinement in the radial directions while displacement of focal planes assures stability in the longitudinal direction. The distinct feature of this trapping geometry is that the particles are trapped in the minimum intensity of the beam, which ensures their minimal heating and perturbation by light which can be important for studies of properties of particles and/or for trapping live cells in air.

In this paper we demonstrate, both theoretically and in experiments, a new strategy for multiple three-dimensional (3D) trapping of absorbing particles in gases with a

unidirectional coherent laser beam by taking advantage of potential wells provided by a speckle pattern [17]. In particular, the recent development of holographic traps [18, 19] and so-called 'dark core bottle beams' with an axial region of zero intensity surrounded by light in all three dimensions [20–23] has attracted lots of attention as their hollow area may enable a large number of particles to be trapped simultaneously.

The speckle pattern of a coherent beam presents an ideal 3D trapping field with multiple traps for micron-sized particles [17]. Indeed, a randomly positioned single speckle has a phase singularity—a point of perfect destructive interference with zero intensity. The energy circulates in the closed loops and the phase varies between 0 and 2π around this point forming a three-dimensional optical vortex [24]. In this work we present theoretical discussion of the transverse and longitudinal dimensions of individual speckles, consider the photophoretic forces in a speckle trap, and determine the laser power required to trap an absorbing particle of particular size, density and optical absorption. Finally, we present experimental results on simultaneous trapping of up to several thousands of carbon particles in a randomly distributed speckle pattern and subsequent analysis of their size distribution and dynamics of trapping [17]. The results show the advantages of the new 3D trapping strategy, which combines the confinement of particles in the dark regions, hence avoiding overheatin,g with the ability to trap a large number of particles in a single unidirectional laser beam.

2. Theory of a speckle trap

2.1. Speckle pattern in the image space

A speckle pattern is a wave intensity pattern produced by the interference of random coherent wavefronts formed by reflectance off or scattering by an irregular surface of the incident wave. The speckle pattern is formed when the surface roughness is high enough to create path length differences exceeding a wavelength, the statistic of the speckle field in this case is independent of the surface irregularities [25, 26]. The resulting wavefront consists of contributions originating from a large number of scattering areas on the surface. If the size of the scattering area is sufficiently small each of those areas can be considered as an independent point source generating an individual elementary wave of coherent light.

The amplitude $U(P)$ of the speckle field at arbitrary point P is given by the sum of elementary monochromatic waves with the amplitudes a_j and phase shifts $\Delta\varphi_j$:

$$U(P) = \sum_{j=1}^{n} a_j \exp(\mathrm{i}\Delta\varphi_j) = A(P)\exp[\mathrm{i}\varphi(P)], \qquad (1)$$

where n is the total number of contributing waves. The resulting amplitude $A(P)$, phase $\varphi(P)$ and intensity $I(P) \sim |U(P)|^2$, all have arbitrary values as a_j and $\Delta\phi_j$ are generated by the stochastic scattering centres. The speckle pattern is well pronounced when the phase shifts are in the range from 0 to 2π. This requires the height Δh_j of irregularities of the scattering surface to be of the order of the wavelength λ as $\Delta\varphi_j \cong (2\pi/\lambda)2\Delta h_j$. The simplest interference pattern at the distance z from the scattering surface is a superposition of waves generated by any two arbitrary points at the surface. The spatial frequency ν of the intensity extreme values in the resulting interference pattern is $\nu = l/\lambda z$, here l is the distance between two points on the surface. The highest spatial frequency, which corresponds to the smallest periodicity in the interference pattern, results from the interference of the farthest points and thus depends on the size of the scattering surface D: $\nu_{\max} = D/\lambda z$. For this reason the minimal speckle size $\varepsilon_{\perp\min}$, which corresponds to a minimal distance between neighbouring intensity maxima in the transverse cross-section is [26],

$$\varepsilon_{\perp\min} = \lambda z/D. \qquad (2)$$

The concept of multiple traps based on the speckle pattern requires careful consideration of the imaging of the scattering surface of a diffuser by an optical system. A spherical wave from a point source is transformed by the imaging system into a converging spherical wave with the centre being an image of the source. The spot spatial structure and the resulting diffraction pattern is determined by the aperture of the imaging system. For a circular aperture of diameter D_a the field amplitude $f(v)$ in the image plane has the form of an Airy function [27]:

$$f(v) = \frac{2J_1(kD_\mathrm{a}\theta/2)}{kD_\mathrm{a}\theta/2}, \qquad k = \frac{2\pi}{\lambda}, \qquad (3)$$

where $J_1(kD_\mathrm{a}\theta/2)$ is the Bessel function, k is a wavenumber, θ is the angular coordinate from the aperture centre and v is the spatial coordinate in the image plane. The radius of the first ring is $\theta_1 = 1.22\lambda/D_\mathrm{a}$. The intensity distribution in the image plane for the point source located on the axis is described by the following function:

$$f(u) = \left[\frac{\sin(u/4)}{u/4}\right]^2; \qquad u = \frac{2\pi}{\lambda}\alpha^2 z, \qquad (4)$$

where α is the angular radius of the aperture from the observation point. The first intensity zero is at the distance $z = \pm 2\lambda/\alpha^2$ from the image plane [27]. The considerations above suggest that the maximum energy density is localized in a cigar-shaped area with the length $l_\mathrm{s} = 4\lambda/\alpha^2$ and width $d_\mathrm{s} = 1.22\lambda/\alpha$. A similar result can be derived for an off-axis source [27].

In the case of several coherent point sources each of them generates an individual diffraction pattern in the image plane. The superposition of these patterns results in a field of isolated spots with the smallest size approximately equal to the diameter of the first diffraction disc formed by the focusing lens aperture from a point source. The speckle pattern emerges when the imaging system is unable to resolve the individual irregularities on the rough surface $d > r_\mathrm{a}$, here r_a is the size of irregularities and d is the resolution size: $d = 1.22\lambda z_0/D_i$, where z_0 is the distance from the source to the imaging aperture and D_i is the diameter of the aperture. Then each point in the imaging plane is a superposition of the coherent waves with a random phase $\Delta\phi_j$, their interference gives rise to the speckle pattern. Assuming a large number of irregularities within

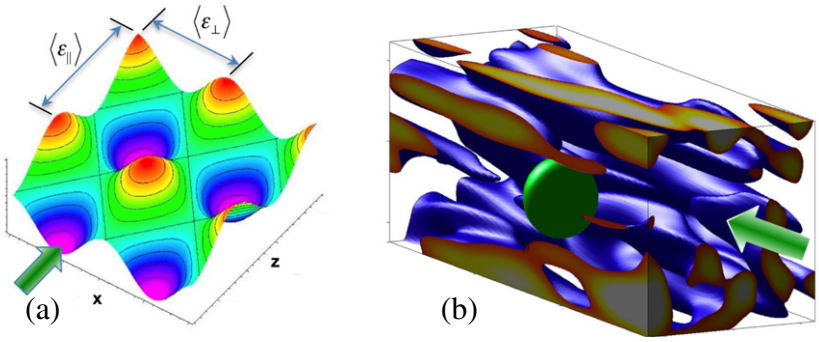

Figure 1. Intensity distribution in a speckle field within the trapping region for the trap parameters $\lambda = 532$ nm, $z_a = 30$ mm, $D_a = 23$ mm. (a) Schematic presentation of intensity distribution in the x–z plane calculated using equations (5) and (6). (b) Numerical 3D modelling of the speckle intensity distribution for a small volume 5 μm × 5μm × 15 μm inside the trapping region with average speckle size of 2 μm in transverse cross-section; a green sphere represents a trapped particle of 2 μm in diameter.

the resolution limit, the speckle pattern can be considered as generated by the aperture limited imaging system with the output lens surface acting as the scattering surface. In this case the speckle pattern is calculated using the imaging system parameters only.

The averaged speckle size is determined in the same way as for a round scattering surface [25] (see figure 1):

$$\langle\varepsilon_\perp\rangle \approx 2.44\lambda z_a/D_a, \tag{5}$$

where z_a is the distance from the output lens surface to the observation plane and D_a is the output aperture diameter. The length of an individual speckle is estimated by the following relation [25, 26]:

$$\langle\varepsilon_\parallel\rangle \approx 16\lambda z_a^2/D_a^2, \tag{6}$$

which coincides with the distance between two intensity minima in the longitudinal cross-section of the Fresnel diffraction pattern generated by a circular aperture of diameter D_a.

Equations (5) and (6) show that in the image area the speckles are elongated along the direction of light propagation, $z > D_a$, $\varepsilon_\parallel > \varepsilon_\perp$. This implies that the intensity distribution in the image space can be envisioned as having isolated randomly arranged local maxima and minima with characteristic scale determined by equations (5) and (6). Consequently, the size of individual cigar-shaped speckles increases with the distance to the image plane.

It is important to note that the contrast of the speckle pattern is equal to unity, i.e. the local intensity minimum is zero [24–26]. In addition, the bright and dark areas in the speckle field are inversely interchangeable owing to their interference nature. What this means is that the above-considered model of elongated cigar-like speckle shape can be applied to both the bright and the dark areas in the light field. For this reason the individual dark region in the speckle field provides ideal conditions for multiple traps for light absorbing particles.

2.2. Forces in the trap

The major force responsible for optical trapping of light absorbing particles in air is the photophoretic force [9–15], F_{ph}, which is much stronger than the radiation pressure in gases, so that the latter can be neglected. As the photophoretic force has to compensate gravity for reliable trapping in air, a necessary condition for stable photophoretic trapping of an absorbing particle with the linear size d_p is [15]:

$$d_p \leqslant \varepsilon_w; \qquad F_{ph} > \frac{\pi}{6}\rho_p d_p^3 g, \tag{7}$$

where ρ_p is the particle density, ε_w is the distance between the neighbouring intensity maxima, and g is the gravitational constant.

The trapping area is the area of maximum laser energy concentration. In the situation of the speckle pattern considered here, this is the diffuser imaging area beyond the focal plane.

The efficiency of trapping, which is the ability to capture and hold particles of particular size with particular laser power, is an important characteristic of the trap. The efficiency of speckle trapping can be determined in the following way. On average, according to [24], each speckle is an individual optical vortex. For this reason the speckle field can be modelled as an average over the ensemble of intensity zeros in Gaussian envelopes separated in space by average transverse and longitudinal dimensions of the speckle, $\langle\varepsilon_\perp\rangle$ and $\langle\varepsilon_\parallel\rangle$. Then the photophoretic force acting in a single-speckle micro-trap can be calculated following the approach of [14, 15]. The photophoretic force vanishes at the minima of the speckle field for a particle with diameter d_p; it should be present, following [15], as

$$F_{ph} \approx \frac{8}{3}\kappa\Delta P_s \frac{R d_p^3}{\langle\varepsilon_\perp^4(z)\rangle}, \tag{8}$$

where d_p is the diameter of the particle, ΔP_s is the laser power in a single speckle, R is the shift of the particle centre from the intensity zero, and κ is a combination of the particle and gas parameters such as the gas viscosity, temperature, and pressure; the particle and gas density and thermal conductivity; and the particle absorption of laser light. The stable trapping condition is $R < \varepsilon_{\perp,\parallel}/2$, which means the deviation of the particle position is less than half of the speckle size. Thus, the

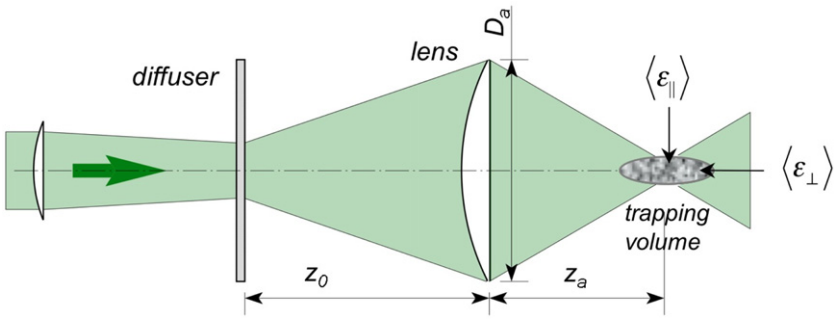

Figure 2. Experimental scheme for generating the speckle-based multiple 3D-traps with a single laser beam.

threshold laser power for trapping from equations (7) and (8) is the following:

$$\Delta P_{\min} \cong \frac{\pi \rho_p \, g \langle \varepsilon_\perp^3 \rangle}{8\kappa}. \tag{9}$$

The laser power in a single speckle is $\Delta P_s = \bar{I} \Delta S$, where $\bar{I}$ is the average intensity over the speckle area, $\Delta S = \pi \langle \varepsilon_\perp \rangle^2 / 4$. A link between the total laser power P and ΔP_s is as follows:

$$P = \sum_1^{N_\perp} \bar{I}_n \Delta S_n = \int_\infty I \, \mathrm{d}S = \text{constant}, \tag{10}$$

where $N_\perp$ is the number of speckles in the beam cross-section, which corresponds to the number of traps N_ε in a single-speckle layer of $\langle \varepsilon_\parallel \rangle$-thickness. The effective trapping occurs in the maximum of the laser energy density in the image area. The speckle size is approximately constant there, however the number of speckles in a single-speckle-thick layer depends on its longitudinal coordinate z: $N_\varepsilon = N_\varepsilon(z)$. Thus, the total number of mini-traps in the trapping area can be obtained as

$$N = \frac{4}{\pi \langle \varepsilon_\perp^2 \rangle} \sum_{i=1}^{N_\parallel} S_i(z), \tag{11}$$

where $N_\parallel = \Delta z / \langle \varepsilon_\parallel \rangle$ is the number of $\langle \varepsilon_\parallel \rangle$-thick layers in Δz distance, and $S_i(z)$ is the area of the ith layer.

It should be mentioned that the trapping conditions derived above can be affected by the presence of strong heat convection (as was seen as the upward motion of particles in the movies in [17]). However, the majority of our experiments described in section 3 have been conducted in the conditions of no noticeable convection in a closed cell. In such a case, when the laser is switched off, the only forces acting on the particle in air are the gravity, which is of the order of 0.5 fN for a 2 μm particle [28], and the buoyancy force acting in the upward direction, which is of the order of 0.07 fN in air for the same particle. The sum of these forces is the driving force, which moves particles predominately down in the absence of the photophoretic force from the laser beam. Diffusion of particles is also negligible as its rate is estimated to be roughly 5 μm s^{-1} in the conditions of the experiment [29, 30], while the experimentally observed rate of particles falling off the trap when the laser is blocked for a part of a second is in the range from hundreds of microns per second to millimetres per second. This observation serves as strong evidence that gravity is the dominant force driving the particles in the absence of laser light and hence will determine the necessary power requirements for trapping.

3. Experiments on multiple trapping

We used a cw laser (Verdi 5 from Coherent, $\lambda = 532$ nm) to form a multiple-pocket trap based on the speckle pattern. The laser light was focused on a ground glass diffuser (Thorlabs DG10-1500) to a 0.5 mm spot, which was further imaged with a lens into a glass cell filled with carbon particles; the experimental scheme is presented in figure 2. The image of the diffuser formed the trapping area consisting of many speckle-originated traps in a glass cell; the size of the area as well as the average speckle size could be varied by using lenses with different numerical apertures and changing the image magnification. The trapping area was observed from a side, showing the scattered laser light by the trapped particles, and along the beam axis through a notch filter using white light injected into the optical path of the trapping beam as a background (figure 3).

Agglomerates of carbon nanoclusters [28, 31, 32] of various sizes and irregular shapes were placed in a glass cell for the trapping experiments. With the laser beam switched on, the particles suspended in air were entering the trapping area through the Brownian motion and were reliably captured in the random speckle traps. The particles could be held in the traps for unlimited time in our experiments—up to 24 h (figure 3(a)). In figures 3(b)–(d) we demonstrate the ability to vary the shape of the trapped area by changing the form of the diffuser illumination. We used a Gaussian beam, a doughnut beam, and a cross shape illuminating the diffuser. As is clearly seen in figure 3, the cloud of trapped particles reproduced the shape of the beam image reasonably well.

We have chosen two lenses L1 and L2 with different D_a/f ratios of 1.21 and 0.37 ($f_1 = 19$ mm and $f_2 = 63$ mm correspondingly, $D_a = 23$ mm for both lenses) to test the dependence of the average speckle size on the size of the trapped particles. The lenses were positioned at different distances from the diffuser $z_{01} = 41$ mm and $z_{02} = 140$ mm so that they form similar trapping volumes at $z_{a1} = 35.4$ mm and $z_{a2} = 114.5$ mm correspondingly (i.e. images of the spot on the diffuser have similar magnifications), but generate different

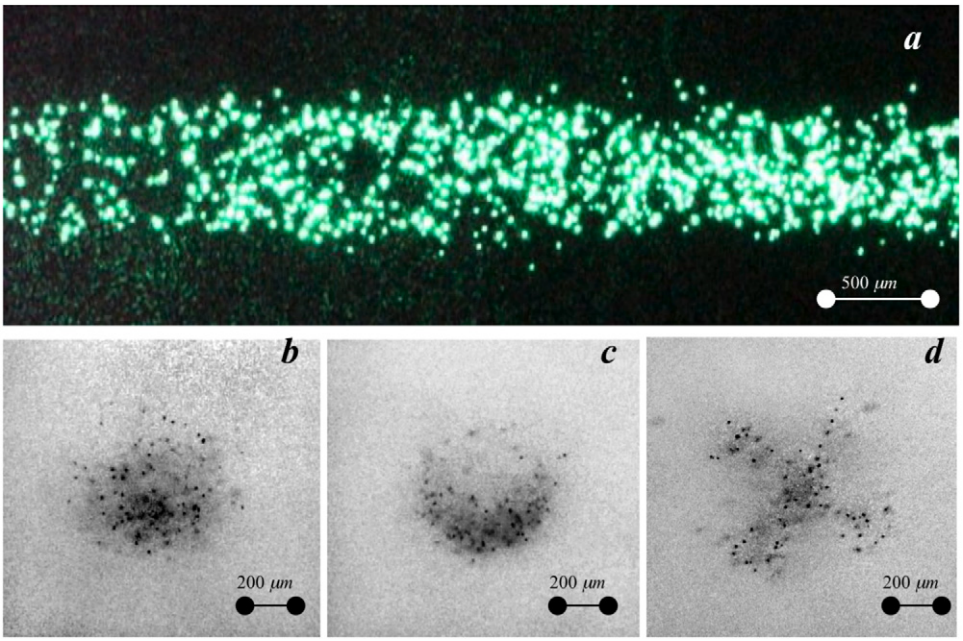

Figure 3. Optical images of the trapped particles: (a) side view of the laser light scattered from thousands of trapped particles; ((b)–(d)) axial views for different beam shapes on the diffuser: (b) a Gaussian beam, (c) a doughnut-like beam, (d) a cross-like beam shape. The total laser power was 115 mW in all these experiments.

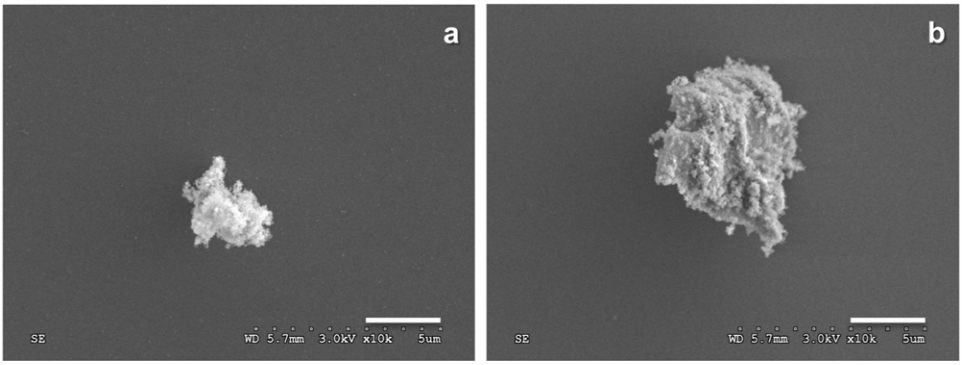

Figure 4. SEM images of typical carbon nanoparticle aggregates collected from the trap on a silicon wafer; the scale bars are 2 μm in both images.

average speckle sizes of 2.0 and 6.4 μm in the transverse cross-section, which is determined by the z_a/D_a ratio—see equations (5) and (6) above. Special care was taken to ensure that the total laser intensity forming the trap of 125 W cm^{-2} was the same in both experiments.

In order to analyse the size of trapped particles, we collected them from the trap on a silicon wafer in the following way. The particles in the cell were disturbed by shaking the cell or by cleaning the cell walls with a fine brush and shaking the particles off the brush. The trapped particles were left for about an hour to ensure that all other particles in the cell were eventually deposited on the cell walls. The trapped particles were then collected on a silicon wafer and analysed under a scanning electron microscope (SEM). Typical SEM images are presented in figure 4 and histograms of the particle size distributions for both traps are shown in figure 5; a total of 460 trapped particles were measured. The measured particle sizes were fitted with Poisson distributions representing independent events also presented in figure 5. The Poisson fittings show the average size of $\langle d_{p1}\rangle = 1.14$ μm for the trap with $\langle \varepsilon_{\perp 1}\rangle = 2.0$ μm and $\langle d_{p2}\rangle = 1.67$ μm for $\langle \varepsilon_{\perp 2}\rangle = 6.4$ μm. (figure 5). The results indicate a tendency for selection of larger, on average, size of the particles trapped with a larger speckle size.

4. Analysis of results

Let us estimate the efficiency of trapping. The total number of traps within the layer with the thickness of the single-speckle length is $N_\perp = d_a^2/\langle \varepsilon_\perp\rangle^2 \cong 1.1 \times 10^5$. On the other hand, according to equation (11) the total number of mini-traps in the trapping volume is $N \approx 10^7$. However, only a few thousand particles were collected and held simultaneously, which means that, on average, only one in 10^4 traps was filled.

The experimentally defined minimal threshold power for the trap with 2 μm average speckle size is $P_{min} = 28.9$ mW,

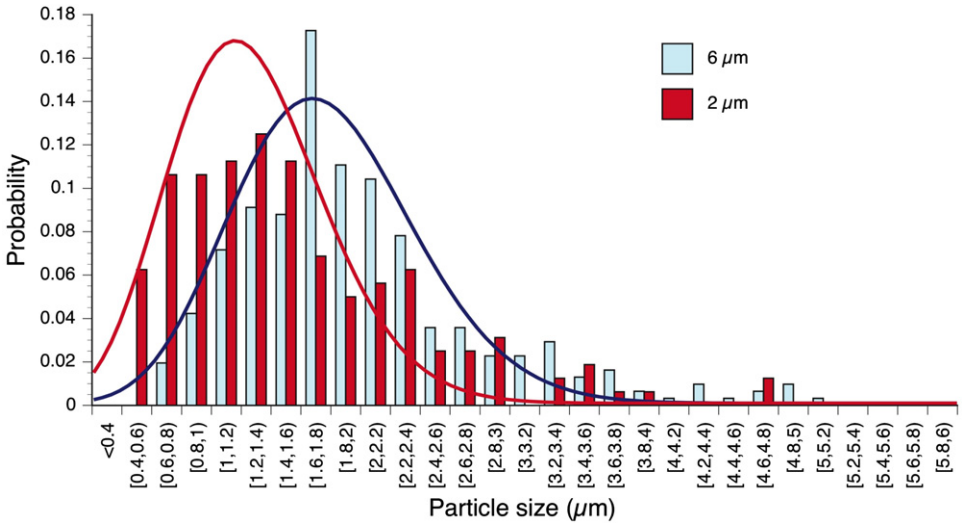

Figure 5. Size distribution of the particles collected from the traps with 2 and 6 μm average speckle size; the size intervals are 0.2 μm. Both histograms were fitted with a Poisson distribution function (solid lines), showing a maximum at 1.14 μm for 2 μm speckles and 1.67 μm for 6 μm speckles.

the total power in the laser beam suggests that the average laser power per single-speckle trap, according to equation (10), is $\Delta P_{\min} = P_{\min}/N_{\perp} \cong 0.3$ μW. By applying equation (9) and taking into account $\kappa = 8.5 \times 10^{-7}$ s m^{-1} [14, 15] and the characteristic mass density of the nanofoam of $\rho_{\mathrm{p}} = 10^{-2}$ g cm^{-3} [30, 31] and $g = 980$ cm s^{-2}, the minimum power per single speckle is $\Delta P_{\min(\mathrm{theor})} \geqslant 3.6$ nW. This estimated threshold value does not take into account convective air flow; it is two orders of magnitude lower than measured in our experiments where the perturbative air flow dominated. The total estimated mass of particles trapped using 125 mW laser power is $\sim 8 \times 10^{-10}$ g, thus the efficiency of trapping in our experiments is $\sim 7 \times 10^{-9}$ g W^{-1}.

To visualize the dynamics of the trap population we process the experimental recordings of a fragment of the trap in real time given in movies 1 and 2 in [17]. Movie 1 shows the gradual population of the trap at fixed power of 115 mW. Because the exposure time of each frame was relatively large, many of the moving particles appeared as long tracks and some of these tracks obscured particles already in the trap. Since particles were trapped in three dimensions, there was also considerable variation in the brightness and apparent size of the particles. This makes application of the particle tracking procedure difficult, as it has to cope with very fast and very slow particles simultaneously. This problem was solved by applying a temporal averaging to the pixels in the movie, which removes the fast moving particles, allowing easy identification and counting of the trapped particles. For each pixel, we define the time averaged intensity,

$$\bar{I}(t) = \frac{1}{2m+1} \sum_{n=-m}^{n=m} I(t+n),$$

where $I(t)$ is the intensity of the pixel at the time t, and the averaging is done in the window of $(2m + 1)$ frames. If a moving particle occupies a particular pixel in a single frame, by taking the average over a small period of time, it is removed from the frame. As the trapped particles are (roughly) stationary, they are unaffected. The moving particles were isolated by subtracting the filtered frame from the original. In this way, we count trapped (stationary) particles in each frame t, the results are presented in figure 6(a). Two sets of data correspond to the two averaging windows, $m = 10, 20$, with little difference between them, thus in the following we use $m = 10$.

Although the separation of slow and fast particles by averaging does simplify the image analysis, there are still the problems of varying particle size and brightness. Additionally, when the particle density becomes very large, it makes it difficult to distinguish between individual particles. To identify particles, an intensity threshold was set and gave a binary image. Particles were then counted automatically as distinct groups of pixels above the threshold, for example the graphs in figure 6(a) were produced with the threshold 150/256. However, the threshold value affects the particle count: if it is set too high, some dimmer particles may not be counted, while if it is set too low the noise may artificially inflate the particle count. Therefore, we performed the count for several thresholds from 130/256 to 220/256 and, in addition, a manual count was obtained from a few selected frames, the results are shown in figure 6(b).

To visualize the dynamics of the trap population we process the experimental recordings in real time given in movies 1 and 2 in [17]. Recorded is a fragment of the trap in a window of observation 2.3 mm wide, which accounts for ~25–30% of the whole trapping volume. The dominant upward moving direction of the particles in the cell is due to the continuous air current during the experiments. When the trap is being populated (the linear part of the graph in figure 6(b)), the number of particles is relatively insensitive to the threshold used and the automated counts are also consistent with two manual counts in the interval. There is a clear trend for the count to decrease as the threshold is increased,

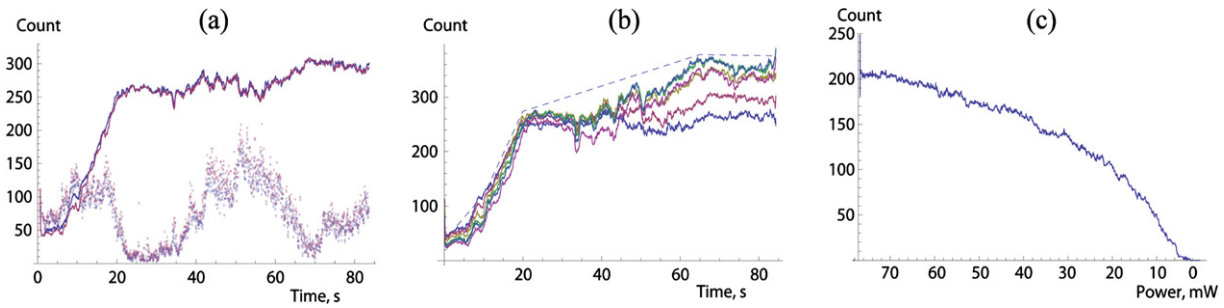

Figure 6. ((a), (b)) Dynamics of trap population, see movie 1 in [17]. (a) Particle count with averaging parameter $m = 10$ (blue online) and $m = 20$ (red online). Lines: number of trapped particles. Points: number of particles moving through the trap. (b) Trapped particle count with different intensity thresholds for particle identification. The dashed line interpolates between manual particle counts at $t = 3.3$, 10, 20, 65 and 84 s. (c) Number of trapped particles as the laser power is decreased continuously for 80 s, see movie 2 in [17]. (Colour online.)

corresponding to the removal of dimmer particles. In the latter portion of the graph, the count is observed to increase with the size of the threshold. Although dimmer particles may be cut out, it appears that the larger threshold makes it easier to distinguish particles which are close together. Beyond a threshold of 210/256 the particle count decreases. The count with thresholds 200/256 and 210/256 may hence be considered a lower bound for the total number of particles in the trap, and they agree reasonably well with two manual counts.

Note that, during the first 20 s, the number of trapped particles increases linearly with time, with the number of particles moving through the trap roughly constant. The interpretation of this is that when the trap is only partially filled, the probability for a particle to get trapped is constant. As the trap fills up, however, not all the moving particles will pass near a vacant micro-trap, so the probability of trapping decreases. Moving particles are also capable of knocking trapped particles out, and these freed particles either keep moving and escape the speckle field or move a short distance before being trapped again. Thus we observe oscillations in the count in figure 6(b).

Finally, figure 6(c) shows the results for the second movie in [17], with the trap depopulated by continuously decreasing the laser power to zero. The same particle identification procedure as above was used. The rate of particle loss increased as the beam power decreased. Since the beam power was continuously decreased in a short time, the power threshold of trapping, mentioned above, is not immediately apparent, as the clearance of the trap below the threshold power requires a certain finite time interval. In other words, when the power is suddenly decreased below $P_{\min}$, some particles still remain trapped, as seen in the movie and the graph in figure 6(c), because some speckles have power much larger than the average. However, these particles also clear from the trap eventually, if the power is fixed in time at any value below $P_{\min}$.

5. Conclusions

In this paper we developed a theoretical basis and demonstrated in experiments a new method for reliable 3D multiple trapping of absorbing particles in air using a mono-directional laser beam. The multiple trapping volume was induced by a speckle pattern which led to a multitude of microscopic-size bottle beams determined by optical singularities in each individual speckle.

There are several important outcomes of this study. Firstly, this work marks the emergence of a possibility for multiple trapping, holding, and sorting, on a large scale of light absorbing particle aerosols in air and other gases, which so far had been beyond the abilities of the standard laser trapping systems. Secondly, the trapping dynamics, and particularly the measured trapping threshold power, makes it possible to determine physical characteristics of the trapped particles, such as thermal conductivity, optical absorption, and density of the microparticles having minute volume and mass. And, finally, the ability to selectively trap, guide and separate suspended particles in air by contactless optical means opens up diverse and rich practical opportunities for laser trapping of matter in a gas environment.

Acknowledgments

We are grateful for the support from the National Health and Medical Research Council and the Australian Research Council.

References

[1] Ashkin A 1970 Acceleration and trapping of particles by radiation pressure *Phys. Rev. Lett.* **24** 156–9
[2] Dholakia K, Reece P and Gu M 2008 Optical micromanipulation *Chem. Soc. Rev.* **37** 42–55
[3] Grier D G 2003 A revolution in optical manipulation *Nature* **424** 810–6
[4] Rubinsztein-Dunlop H, Nieminen T A, Friese M E J and Heckenberg N R 1998 Optical trapping of absorbing particles *Adv. Quantum Chem.* **30** 469–92
[5] McGloin D, Burnham D R, Summers M D, Rudd D, Dewar N and Anand S 2008 Optical manipulation of airborne particles: techniques and applications *Faraday Discuss.* **137** 335–50
[6] Rudd D, López-Mariscal C, Summers M, Shahvisi A, Gutiérrez-Vega J C and McGloin D 2008 Fiber based optical trapping of aerosols *Opt. Express* **16** 14550–60

[7] Beresnev S, Chernyak V and Fomyagin G 1993 Photophoresis of a spherical particle in rarefied gas *Phys. Fluids* A **5** 2043–52
[8] Pluchino A B 1983 Radiometric levitation of spherical carbon aerosol particles using a Nd:YAG laser *Appl. Opt.* **22** 1861
[9] De Nicola S, Finizo A, Mormile P, Pierattini G, Martellucci S, Quartieri J, Bloisi F and Vicari L 1988 Experimental results on the photophoretic motion and radiometric trapping of particles by irradiation with laser light *Appl. Phys.* B **47** 247–50
[10] Lewittes M, Arnold S and Oster G 1982 Radiometric levitation of micron sized spheres *Appl. Phys. Lett.* **40** 455–7
[11] Yalamov Yu I, Kutukov V B and Shchukin E R 1976 Motion of a small aerosol particle in a light field *J. Eng. Phys.* **30** 648
[12] Davis E J and Schweiger G 2002 *The Airborne Microparticle: Its Physics, Chemistry, Optics, and Transport Phenomena* (Heidelberg: Springer) pp 780–5
[13] Steinbach J, Blum J and Krause M 2004 Development of an optical trap for microparticle clouds in dilute gases *Eur. Phys. J.* E **15** 287–91
[14] Shvedov V G, Desyatnikov A S, Rode A V, Krolikowski W and Kivshar Yu S 2009 Optical guiding of absorbing nanoclusters in air *Opt. Express* **17** 5743–57
[15] Desyatnikov A S, Shvedov V G, Rode A V, Krolikowski W and Kivshar Y S 2009 Photophoretic manipulation of absorbing aerosol particles with vortex beams: theory versus experiment *Opt. Express* **17** 8201–11
[16] Nye J F and Berry M V 1974 Dislocations in wave trains *Proc. R. Soc.* A **336** 165–90
[17] Shvedov V G, Rode A V, Izdebskaya Ya V, Desyatnikov A S, Krolikowski W and Kivshar Yu S 2010 Selective trapping of multiple particles by volume speckle field *Opt. Express* **18** 3137–42
[18] Dufresne E R, Spalding G C, Dearing M T, Sheets S A and Grier D G 2001 Computer-generated holographic optical tweezer arrays *Rev. Sci. Instrum.* **72** 1810–6
[19] Polin M, Ladavac K, Lee S H, Roichman Y and Grier D G 2005 Optimized holographic optical traps *Opt. Express* **13** 5831–45
[20] Arlt J and Padgett M J 2000 Generation of a beam with a dark focus surrounded by regions of higher intensity: the optical bottle beam *Opt. Lett.* **25** 191–3
[21] Bokor N and Davidson N 2007 A three-dimensional dark focal spot uniformly surrounded by light *Opt. Commun.* **279** 229–34
[22] Shvedov V G, Izdebskaya Ya V, Desyatnikov A S, Rode A V, Krolikowski W and Kivshar Yu S 2008 Generation of optical bottle beams by incoherent white-light vortices *Opt. Express* **16** 20902–7
[23] Steuernagel O 2005 Coherent transport and concentration of particles in optical traps using varying transverce beam profiles *J. Opt. A: Pure Appl. Opt.* **7** S392–8
[24] O'Holleran K, Dennis M R and Padgett M J 2009 Topology of light's darkness *Phys. Rev. Lett.* **102** 143902
[25] Goodman J W 2007 *Speckle Phenomena in Optics* (Greenwood Village, CO: Ben Roberts)
[26] Vest C M 1979 *Holographic Interferometry* (New York: Wiley)
[27] Born M and Wolf E 2003 *Principles of Optics* 7th edn (Cambridge: Cambridge University Press) Expanded
[28] Rode A V, Gamaly E G and Luther-Davies B 2000 Formation of cluster-assembled carbon nano-foam by high-repetition-rate laser ablation *Appl. Phys.* A **70** 135–44
[29] Jovanovic O 2009 Photophoresis—light induced motion of particles suspended in gas *J. Quant. Spectrosc. Radiat. Transfer* **110** 889–901
[30] Rohatschek H 1995 Semi-empirical model of photophoretic forces for the entire range of pressures *J. Aerosol Sci.* **26** 717–34
[31] Rode A V, Elliman R G, Gamaly E G, Veinger A I, Christy A G, Hyde S T and Luther-Davies B 2002 Electronic and magnetic properties of carbon nanofoam produced by high-repetition-rate laser ablation *Appl. Surf. Sci.* **197/198** 644–9
[32] Lau D W M, McCulloch D G, Marks N A, Madsen N R and Rode A V 2007 High-temperature formation of carbon onions within nanofoam: an experimental and simulation study *Phys. Rev.* B **75** 233408